Photocatalytic activity of electrophoretically deposited (EPD) TiO_2 coatings

Manuel Nuño[1], *Richard J. Ball*[1*], *Chris R. Bowen*[2]*: Rajnish Kurchania*[3]*: G. D. Sharma*[4]

[1] BRE Centre for Innovative Construction Materials, Department of Architecture and Civil Engineering, University of Bath, Claverton Down, BA2 7AY

[2]Department of Mechanical Engineering, University of Bath, Claverton Down, BA2 7AY

[3] Department of Physics, Maulana Azad National Institute of Technology (MANIT) Bhopal 462051, Madhya Pradesh, India

[4]Jaipur Engineering College (JEC) Jaipur 303101, Rajasthan, India

* Corresponding author

Abstract

This paper describes the application of electrophoretic deposition for air pollution removal using anatase as a photoactive coating. In this study the anatase form of TiO_2 has been applied to (i) fluorine-doped tin oxide coated glass; (ii) 304L stainless steel; and (iii) titanium substrates using isopropanol and acetylacetone based solutions at 20, 40, 60 and 80V. In order to increase the strength of the substrate-anatase interface without transforming the phase into rutile, samples were calcined at 450ºC for 2 hours. The resulting coatings were characterised by Raman spectroscopy, X-ray diffraction (XRD), non-contact optical profilometry and scanning electron microscopy (SEM). The photocatalytic activity of the deposited coatings were evaluated in the gas-phase for nitrogen dioxide (NO_2) removal by electron ionisation mass spectrometry whilst irradiated by light of wavelength 376-387nm for 100 minutes. Anatase phase titania supported on a fluorine-doped tin oxide coated glass substrate showed the highest photoactivity for NO_2 remediation. This was attributed to the formation of a three-dimensional nanostructure with properties determined by the deposition conditions. The work provides routes for the development of low-cost and large area photoactive coatings for pollution control.

Keywords electrophoretic deposition, photocatalysis, TiO_2, anatase, NO_2, mass quadrupole

Abbreviations

a.m.u. = atomic mass unit

FTO = fluorine doped tin oxide

CH_4 = methane

NO_x = nitrogen oxide

UVA = ultraviolet-A

1. Introduction

The latest assessment report by the Intergovernmental Panel on Climate Change released in March 2014 indicated the required actions for the mitigation of climate change [1]. The release of greenhouse gases such as carbon dioxide, methane, sulphur dioxide and nitrous oxide from industrial and domestic sources pose a significant contribution to global warming. Many of these gases also present health hazards for the population at large and are associated with respiratory diseases. The European Union and United States of America have set maximum levels for emissions of certain pollutants through their environmental standards; the levels for SO_2 were set in 2005 and NO_2 in 2010[2].

In 1972 Fujishima and Honda first published their research on the photocatalytic properties of TiO_2 [3]. Greater awareness of the potential ways to exploit the photoactivity of semiconductors such as titanium dioxide has seen a significant increase in the quantity of research investigations carried out. This has been largely driven by their promise of becoming a method for pollution remediation [4]. Under UV radiation, semiconductors with photocatalytic activity can create free radicals on their surface. This process begins [3], [5–7] with the promotion of electrons from the valence to the conduction band. Following charge separation, the creation of a reactive hole (h_{vb}^{+}) on the surface of the crystal and the associated electron are able to interact with surface adsorbed water molecules generating free hydroxyl radicals and protons. The charge-separation reaction scheme is illustrated by equations 1 to 6 [8–11], starting with the initial creation of electron hole pairs on the TiO_2 surface (Reaction 1) prior to the creation of free radicals. Free radicals are responsible of the reduction-oxidation (redox) processes associated with the neutralisation and subsequent removal of hazardous molecules. Although titanium dioxide has three different metastable polymorphs, anatase with a band gap of 3.2eV [12], [13] is widely accepted as being the most efficient structure for separating charges on its surface under UV radiation [14] and is therefore considered more reactive against pollutants compared to the other polymorphs of TiO_2 such as rutile and brookite.

The photocatalytic activity of various materials is routinely studied for powders or nanoparticles whilst in the form of an aqueous suspension. Under these conditions the decomposition rate of a suitable organic dye, such as methylene blue, is used as a measure of activity [15–23]. This simple method was subsequently standardized in ISO (International Organization for Standardization) 10678. However the physical mechanisms involved in such aqueous based methods can be significantly different compared to that of gas-phase reactions making the translation of relative performance problematic. There are currently three published ISO methods related to air purification, each one being specific to one pollutant: acetaldehyde (CH_3CHO) ISO 222197-2; nitric oxide (NO) ISO 22197-1 and toluene ($CH_3C_6H_5$) ISO 22197-3. A chromatographic system is commonly used as the detector, however this has the disadvantage of being limited to one compound [24]. Recent developments in the application of electron ionisation mass spectrometry for the study of photo-catalytic activity has demonstrated the

suitability and reliability of this approach for multiple pollutants. Studies have differentiated between rutile and anatase forms of TiO_2 under irradiation at different wavelengths in the UVA range [25].

$$TiO_2 + h\nu \rightarrow h_{vb}^{+} + e_{cb}^{-} \quad (1)$$

$$h_{vb}^{+} + H_2O \rightarrow \bullet OH + H^{+} \quad (2)$$

$$e_{cb}^{-} + H^{+} \rightarrow \bullet H \quad (3)$$

$$e_{cb}^{-} + O_2 \rightarrow O_2^{\bullet -} \quad (4)$$

$$h_{vb}^{+} + O_2^{\bullet -} \rightarrow {}^1O_2 \quad (5)$$

$$H^{+} + O_2^{\bullet -} \rightarrow HO_2^{\bullet} \quad (6)$$

The development of photocatalytic paints and coatings for environmental remediation applications in both indoor and outdoor urban areas has been identified as a promising field of research [26–31]. In this study, electrophoretic deposition of nanostructured anatase TiO_2 coatings on stainless steel, titanium and fluorine-doped tin oxide coated glass substrates have been investigated. These substrates are widely used by the construction industry for structural and esthetical applications in buildings. Many of the associated components are pre-fabricated and potential candidates for coating using electrophoretic deposition.

Electrophoretic deposition is a versatile technique which has seen widespread use over the last 50 years. It is suitable for coating a wide range of materials including carbides [32], ceramic oxides [33], [34], metals [35] and polymers [36] onto an electrically conducting surface. When an electric field is applied to the solution, the charged particles are accelerated towards the electrode with opposite polarity. Additives can be added to the solvent mixture to modify the electrical conductivity of the media and provide charge stabilisation of the suspended particles [34], [37]. Studies by Boccaccini, Farnoush, Mohanty, Caya and Fateminia have investigated a number of different solvents suitable for electrophoretic deposition of metal oxides[38–42]. Those based on isopropanol and acetylacetone were identified as producing coatings with high durability and uniformly deposited oxide nanoparticles. This is attributed to physical properties including the dielectric constant, 18.6 and 23.1 at 20°C, viscosity index, 2.4 mPa.s and 0.821mPa.s at 20°C for isopropanol and acetylacetone respectively.

Electrophoretic deposition has also been employed by industry as a material processing technique for coating automobile frames, heavy equipment and metal parts [37], [43]. It is particularly appropriate

for components with complex geometries where other methods may produce unacceptable variations in coating thickness [44]. An additional advantage of this technique includes a relatively rapid processing speed and lower costs when compared to alternative methods such as sol-gel processing. Electrophoretic deposition has been shown to produce coatings of sufficient quality for use in the production of dye-sensitized solar cells. It is well suited for the production of the high purity coatings required for such applications[44–47].

This paper describes a study to investigate the photocatalytic performance of electrophoretically deposited coatings through testing their ability to remove NO_2 from air. The effect of deposition parameters including suspension medium, voltage, current and time have been investigated for glass and metal substrates to optimise the coating durability and photocatalytic activity. The research demonstrates the suitability of this technique which could be scaled-up and used for the production of large area photocatalytic coatings for the built environment in common materials used in facades such as glass, steel and titanium.

2. Material and methods

a. Preparation of anatase TiO_2 coatings

Nanostructured coatings were formed from an anatase precursor supplied by Sigma Aldrich and marketed as Aeroxide® P25 of purity ≥99.5% trace metals basis, average particle size 21nm, a surface area ranging from 35m^2/g to 65m^2/g and a thermal expansion coefficient of 8.4×10^{-6}/K CAS 13463-67-7. The three electrically conductive substrate materials that were evaluated were (i) stainless steel of grade AISI 304L (sections 25mm x 25mm x 1.00mm) with an electrical resistivity of 7.2×10^{-5}Ωcm at 20°C and a thermal expansion coefficient of 1.7×10^{-5}/K; (ii) 99.6% purity titanium sheet supplied by Advent Research Materials Ltd. (sections 25mm x 25mm x 1.00mm) with an electrical resistivity of 4.2×10^{-5}Ωcm at 20°C and a thermal expansion coefficient of 8.6×10^{-6}/K and (iii) soda glass coated in a conductive fluorine doped tin oxide film of sheet resistance 8Ω/sq and a thermal expansion coefficient of 9×10^{-6}/K was supplied by Visiontek Systems Ltd (sections 25mm × 25mm × 3.20mm). Prior to deposition, all substrates were ultrasonicated in deionised water for 15 minutes, washed in acetone to remove surface contaminants and subsequently air-dried using a hot air blower. Electrophoretic deposition (EPD) was carried out using either an isopropanol based solution which consisted of 30 ml of isopropanol, 15 ml of acetone and 0.5 ml of acetylacetone, 0.1% w/v of iodine and 1% w/v of anatase, or an acetylacetone based solution which consisted of 30ml of acetylacetone, 0.1% w/v of iodine and 1% w/v of anatase. Following the addition of these constituents intimate mixing was ensured by ultrasonicating the solution for 15 minutes prior to deposition.

Electrophoretic deposition was performed in a specially designed and constructed cell containing a platinum counter electrode (section of 1.00mm x 2.50 x 0.50mm) with an inter electrode distance of 2.7 cm. A Keithley model 2400 power supply with a voltage range of 5μV to 210V, programming resolution

of 5mV and maximum power of 22W was used. The basic accuracy at 23°C ± 5 °C was 0.012% of the reading voltage ± 24mV. The noise, peak to peak, between 0.1 and 10 Hz was 5 mV. As-prepared samples were dried at room temperature and were then calcined in a conventional furnace. The temperature was ramping up at 1°C per minute to 450°C and the dwell time at the final temperature was 2 hours. The coatings were naturally cooled to room temperature. In addition to the coatings, a 13mm diameter anatase P25 pellet was formed by dry cold pressing, at a pressure of 69 kN/m^2 for use as a reference.

b. Evaluation of NO_2 photodegradation

Photocatalytic activity of the coatings in the solid-gas phase was studied within a stainless steel reaction chamber connected to a quadrupole mass spectrometer via a leak valve. Irradiation of the sample within the chamber was achieved through a quartz glass window using a 4 x 4 array of UV LED's of wavelength 376-387nm. The gas mixture studied comprised 190ppm of NO_2, 6% of air balance N_2, and this composition was used for all the experiments.

The rate of degradation ratio was measured by Microvision 2, a mass spectrometer provided by MKS Instruments Inc. which worked with an emission current of 1mA, the electron energy was set to 70eV, an ion energy of 5.5mA, and a scanning range from 14m /z to 70m /z with a step size of 0.12m /z scanning 8 points per a.m.u.

Under these conditions two separate experiments were undertaken, in the dark and under a UV LED of wavelength 376-387nm. In addition to the experiments carried out with a sample inside the reaction chamber, control experiments were performed without a sample inside the chamber and with no light irradiation; these are referred to as '*dark no sample'*. In all the cases the experiments were performed over a period of 100 minutes.

The data treatment applied to the measurements has been previously reported in detail [24] and consists of a multiplicative approach which reports the fractional changes of NO_2 and compares it to that of an inert internal standard, Ar, considering the shape of the curve for the partial pressure of an element irrespective of the absolute pressure. The fractional change of Ar during the experiment is defined as α, where the superscript 'max' is the maximum value of its partial pressure for the data series; 'min' is the minimum value of its partial pressure for the data series and 'i' is the partial pressure value for a given time during the experiment.

$$\alpha = \frac{Ar^{max} - Ar^{i}}{Ar^{max} - Ar^{min}} \qquad (7)$$

This treatment can be applied using similar methodology to the data relating to the m/z ratio of a molecule of interest, in this case NO_2.

$$\varepsilon_{NO_2} = \frac{{NO_2}^{max} - {NO_2}^{i}}{{NO_2}^{max} - {NO_2}^{min}} \quad (8)$$

ε_{NO2} represents the relative change in signal from the NO_2 molecule. This treatment normalises the data to a value between 0 and 1. The fractional change of nitrogen dioxide, ${}^{i}_{N}NO_2$, is then calculated relative to the change of argon, α. The difference in active surface area between different samples is considered by dividing by the surface area, A, as shown in equation 11.

$${}^{i}_{N}NO_2 = \frac{\varepsilon_{NO_2} - \alpha}{A} \quad (9)$$

After 100 minutes, the fractional change value of NO_2 for the reaction under UV was subtracted from the fractional change value of NO_2 with no sample in the chamber.

c. Characterization of the anatase coatings

X-ray diffraction and Raman spectroscopy were used to determine the phase composition of the coatings. XRD was carried out using a BRUKER D8 ADVANCE X-ray diffractometer with CuK_α radiation, 2θ with a step of 0.016° and a step time of 0.269s between 20° and 70°. Raman spectroscopy was performed using a Renishaw inVia Raman microscope with a motorised sample stage and 532nm SHG Nd:YAG laser. The homogeneity of the crystal phases within the coating was determined by mapping a 1000μm by 500μm area. This was performed using Wire 4.1 software which controlled positioning along the x-y plane, with the ability to scan a region using an objective lens with a magnification of 50x. Dimensional surface measurements by non-contact optical profilometry were performed using a Proscan 2000 with a chromatic sensor with a resolution of 0.01μm. The morphology of the coatings was evaluated at low magnifications using a VHX-5000 Digital optical microscope equipped with a CMOS image sensor (virtual pixels: 1600 (H)x x1200(V)) provided by Keyence. Higher magnification images were obtained using a JEOL JSM64802V scanning electron microscope (SEM) with an accelerator voltage of 10kV and a spotsize of 25nm. Where necessary the samples were coated with a 10nm film of chromium to prevent charging. Coating thickness was calculated from an average of three measurements taken from an SEM image of a cross-section.

3. Results and discussion

The optimum coating conditions were investigated by systematically changing the exposure time, solvent, voltage and substrate material. These four physicochemical parameters affect the EPD kinetics and were studied through a series of experiments.

The *deposition voltage* and *substrate* influence the electric field in the solution, affecting the particle charge and thus the stability of the suspension [44], [48–51]. The nature of the s*olvent* affects the efficient dispersion of nanoparticles and the deposition of those particles on the substrate [48], [49]. Carrying out the deposition process for longer durations leads to a greater thickness of the coating [49], [51–53]. The conditions applied for each of the four parameters are detailed in the following sections.

a. Effect of deposition time

High exposure time implies a greater coating thickness, however a critical thickness was identified at which point the coating became unstable and cracks formed on the surface after calcination. Exposure sequences during EPD investigated were: 5s, 10s, 30s, 50s, 100s, 300s, 500s, 900s and 1200s.

Figure 1a shows the effect of deposition time for stainless steel and FTO coated glass in acetylacetone based solution deposited at 80V. All the coatings prepared at 80V for 500s failed during the calcination process because of the large number of cracks in the thicker coatings, which is attributed to the stress caused by thermal mismatch between the coating and the substrate.

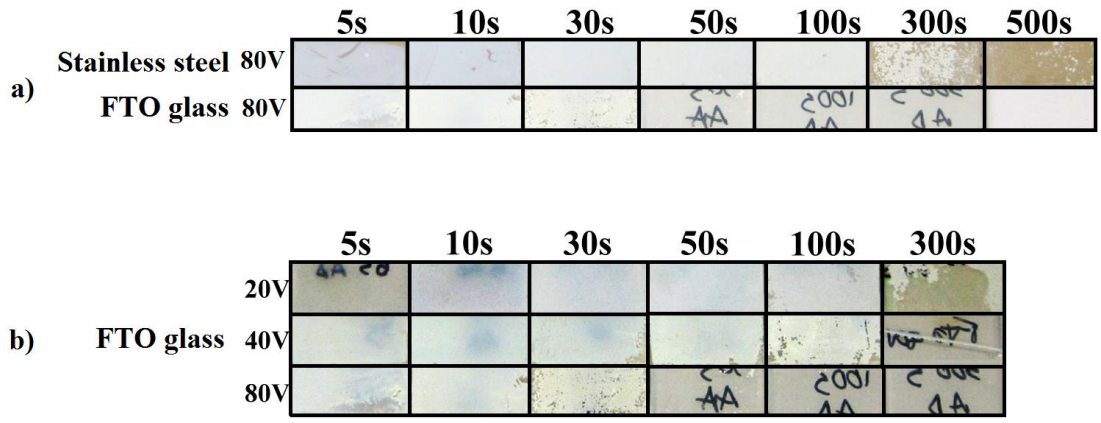

Figure 1 - a) Images of TiO_2 films that were electrophoretically prepared in acetylacetone based solution at 80V after calcination; b) Images of TiO_2 coated FTO coated glass electrophoretically prepared in acetylacetone based solution at 20V, 40V and 80V after calcination.

As shown in Figure 1a, stainless steel was successfully coated with an exposure time under 50, whereas FTO coated glass was successfully coated under 30s. Figure 1b shows the evolution of the deposited

coatings on FTO coated glass that was electrophoretically prepared in acetylacetone based solution at 20V, 40V and 80V at different time sequences. Higher voltages required less time to deposit an anatase coating whereas at a lower voltage of 20V longer exposure times are required to obtain a uniform thickness. The transparent FTO glass samples were labelled on their reverse side using black permanent marker pen and this writing is clearly visible on the thinly coated samples and provides a useful visual indication of the coating thickness.

b. Effect of applied voltage

It is well known that the thickness of the resultant coating is proportional to the applied voltage and the deposition time [51–53]. To study the effect of the voltage and time, the substrate and solvent were fixed (FTO coated glass was used for the substrate in an acetylacetone based solution). As Figure 1b shows, at 20V a uniform coating requires a 50s deposition time whereas, at 40V a 30s deposition time is required and at 80V a 10s deposition time is sufficient to provide a uniform and stable coating. Coatings prepared for durations over 100s produced poorly adhered coatings following the drying and calcination stage of the process.

c. Effect of substrate

FTO coated glass, titanium and stainless steel substrates were used to evaluate deposition voltages of 20V, 40V and 80V for 900s as shown in Figure 2a. The deposition time was chosen to ensure the coating formation achieved the maximum thickness; but only the metallic substrates were coated successfully at 20V, showing a similar behaviour between stainless steel and titanium. Figure 2b shows another experiment performed under the same conditions of voltage and solvent, but with different time exposures for FTO coated glass and stainless steel (as a representative metallic sample). FTO coated glass requires less exposure time to be coated than stainless steel, whereas coatings formed on stainless steel remained stable after exposure times of 100s and 300s. Considering the stability of the coatings after calcination, FTO glass and stainless steel showed the highest adhesion to the substrate-TiO_2. This was attributed to the thermal expansion coefficient´s of FTO coated glass being closest to TiO_2 anatase, reducing thermal mismatch stresses generated during the calcination process.

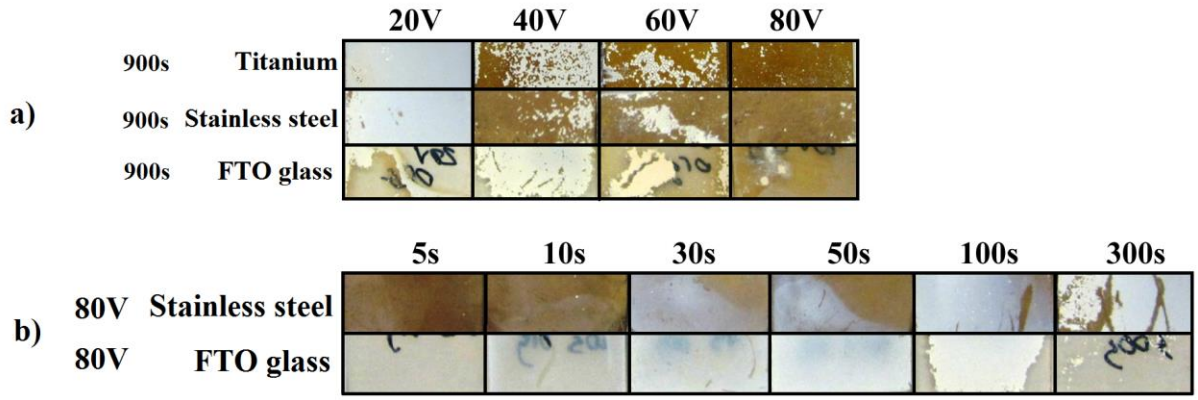

Figure 2 – a) Images of TiO_2 films coated at 20V, 40V, 60V and 80V under isopropyl based solution in three different substrates; titanium plate, stainless steel plate, FTO plate; (b) Images of TiO_2 films coated at 80V under isopropyl based solution on stainless steel plate and FTO coated glass substrates.

d. Effect of solvent

As described in the experimental methods, both isopropanol based and acetylacetone based solutions were used. Figure 3 shows the difference between coatings obtained electrophoretically at 80V in isopropanol and acetylacetone based solutions for a stainless steel substrate. The acetylactone based solution yields a coating with greater uniformity over a wider range of times compared to the isopropyl solution. This is due to acetylactone´s physical and electrical properties, low viscosity and high dielectric constant increasing the mobility of charged particles in the solution. A comparison with FTO coated glass can be made by referring to Figure 4 (bottom two rows). Similar to the steel, the acetylacetone solution gave a better coating on FTO compared to the isopropyl solution, however this was only observed at 5s and 10s indicating that the steel yielded more consistent coatings at short deposition times.

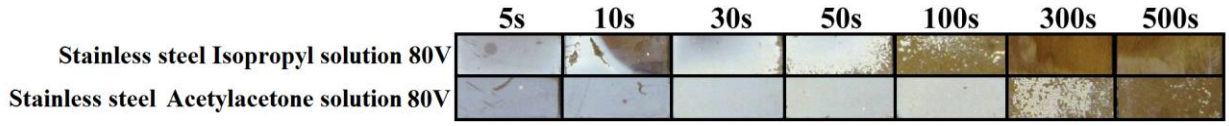

Figure 3 – Images of TiO2 films coated stainless steel at 80V under isopropyl based solution and acetylacetone based solution

Figure 4 shows the differences when the deposition voltage is reduced from 80V to 20V using these solutions on an FTO glass substrate. In all cases the acetylacetone based solution was the most effective solvent forming a uniform and stable TiO_2 coating under high voltages or longer deposition times.

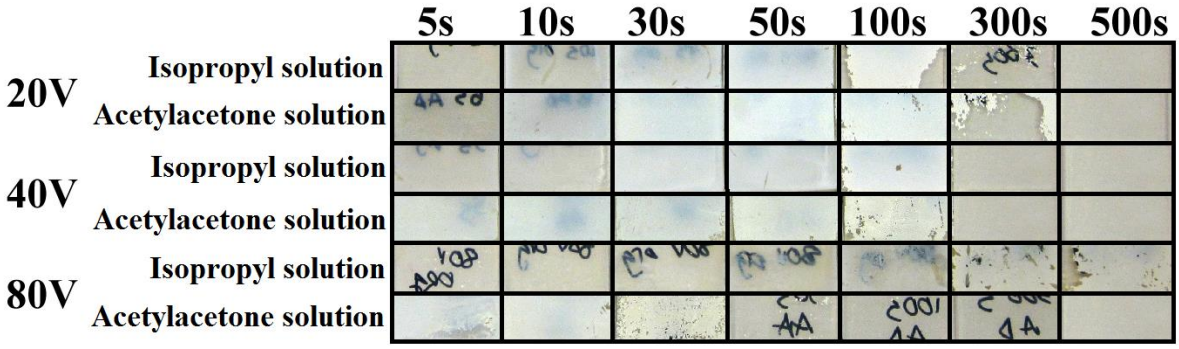

Figure 4 – Images of TiO2 films coated FTO coated glass at 20, 40 and 80V under isopropyl based solution and acetylacetone based solution

e. Surface morphology

Following careful examination of all the samples manufactured the ten coatings (samples a-j) with the most uniform and coherent coatings were subjected to further testing and analysis. Table 1 shows the experimental conditions for each of these coatings and Figure 5 shows representative images taken using an optical microscope.

Table 1 – Parameters used for anatase TiO2 electrophoretically deposited

ID	Substrate	Voltage (V)	Solvent	Time (s)
a	FTO coated glass	20	Acetylacetone based solution	30
b	FTO coated glass	20	Isopropanol based solution	50
c	FTO coated glass	40	Acetylacetone based solution	10
d	FTO coated glass	40	Isopropanol based solution	50
e	FTO coated glass	80	Acetylacetone based solution	10
f	Stainless steel	20	Isopropanol based solution	900
g	Stainless steel	20	Isopropanol based solution	100
h	Stainless steel	80	Acetylacetone based solution	30
i	Stainless steel	80	Acetylacetone based solution	50
j	Titanium plate	20	Isopropanol based solution	900

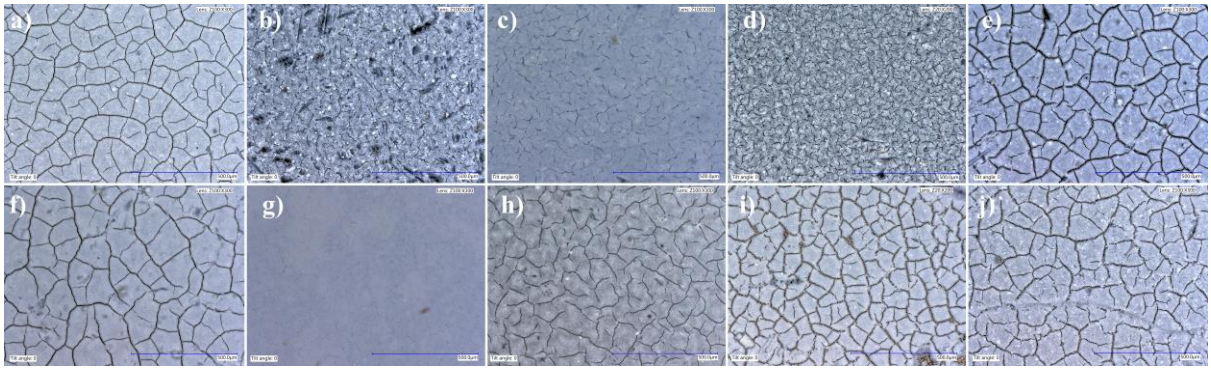

Figure 5 – Images of the TiO2 coatings listed in Table 1

The phase composition of the coatings was determined using X-ray diffraction and Raman spectroscopy as presented in Figures 6 and 7. Figure 6 shows the XRD pattern of the initial anatase P25 and the coating produced by electrophoretic deposition on FTO coated glass at 20V for 50s in an isopropanol based solution. Anatase was confirmed as the predominant phase in P25, as expected, however the presence of rutile was also indicated by a number of peaks. Peaks for both of these phases corresponding to the standard JCPDS XRD data files for anatase (JCPDS No. 21-1272) and rutile (JCPDS No. 21-1276). The XRD pattern of the coating produced by electrophoretic deposition on FTO coated glass was typical of all the coatings characterised and showed the same peaks for the anatase crystal phase with traces of the rutile crystal phase. In addition, in the case of the FTO coated glass, peaks corresponding to SnO_2 from the conductive fluorine doped SnO_2 coating were also observed [54], [55] (JCPDS-041-1445). A comparison of the raw P25 spectra with that of the coatings confirmed that during the coating and annealing process, anatase did not transform into rutile.

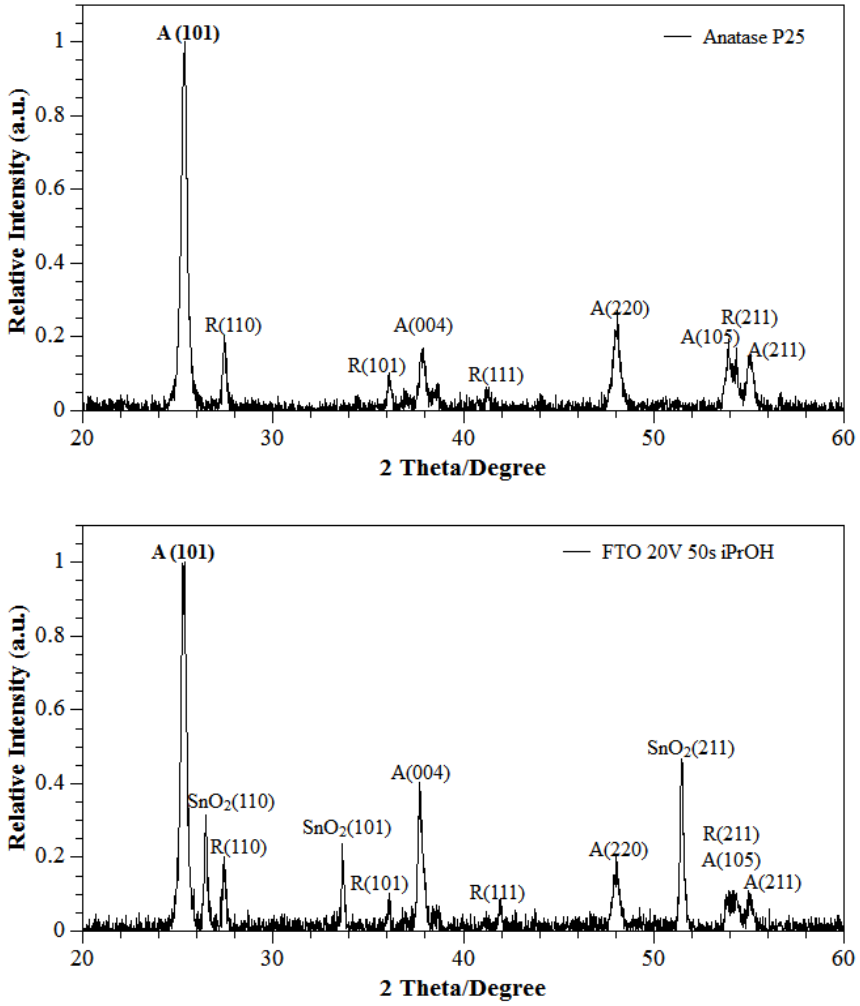

Figure 6 – XRD Spectra of TiO_2 anatase P25 and a typical XRD spectrum of the films (in this case, FTO doped glass coated at 20V for 50 seconds in isopropanol based solution). R=Rutile, A=Anatase

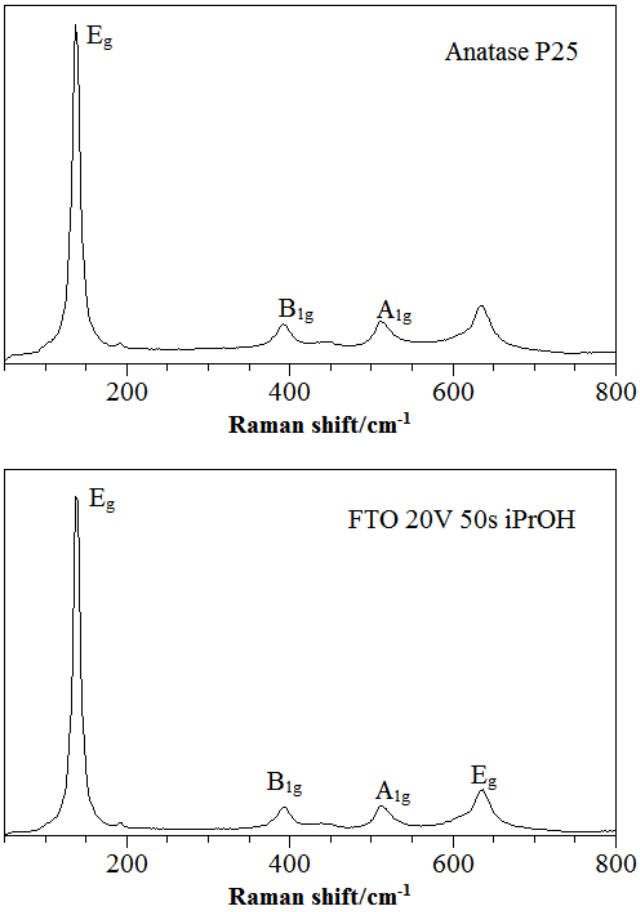

Figure 7 – Raman spectra of anatase P25 (top) and the characteristic Raman spectra TiO_2 coatings produced by electrophoretic deposition for all the films

Figure 7 shows the Raman spectra of anatase P25 and the typical Raman spectra of the coated substrates. Anatase shows four main peaks, 138 cm^{-1} (100% relative intensity), 392 cm^{-1} (11% relative intensity), 513 cm^{-1} (12% relative intensity) and 636 cm^{-1} (17% relative intensity). Two different coatings representative of the deposition methods were identified for study by surface mapping. TiO_2 deposited on titanium foil for 15 minutes in isopropanol based solution at 20V, which represented a metallic coating at a long deposition time; and TiO_2 supported on FTO coated glass for 50s which represented a coating grown on FTO coated glass formed for a short period of time. The results extracted from the data revealed anatase as main component of the surface coating.

To study the three-dimensional morphology of the surface, samples were analysed using a Proscan 2000. Figures 8 shows an example for sample (j) and Table 2 shows the surface texture; average roughness, mean peak to valley height, root mean square average roughness and the thickness for all the coatings. The data shows consistent average roughness values, with coatings deposited at 80V with

high roughness values between 1.21 and 1.84µm, in comparison those produced at 20V or 40V which had lower roughness' between 0.56 and 0.88µm. The coatings thicknesses were however not only influenced by the voltage, but also the deposition time, where longer times resulted in thicker coatings.

Table 2 – Profile roughness parameters and thickness for the studied coatings

ID	Substrate	Based solution	Voltage	Time	Average roughness (µm)	Mean peak to valley height (µm)	Root mean square average roughness (µm)	Thickness (µm)
a	FTO	Acetylacetone	20V	30s	0.77	3.11	0.99	16.4
b	FTO	Isopropanol	20V	50s	0.56	5.14	0.77	12.2
c	FTO	Acetylacetone	40V	10s	0.75	3.40	0.96	7.3
d	FTO	Isopropanol	40V	50s	0.72	3.09	0.92	6.0
e	FTO	Acetylacetone	80V	10s	1.21	4.92	1.80	14.5
f	Steel	Isopropanol	20V	900s	0.88	3.40	1.13	11.9
g	Steel	Isopropanol	20V	100s	0.81	3.22	1.12	9.0
h	Steel	Acetylacetone	80V	30s	1.33	6.78	2.13	18.2
i	Steel	Acetylacetone	80V	50s	1.84	7.95	3.61	22.3
j	Titanium	Isopropanol	20V	900s	0.84	3.95	1.28	15.1
k	Pellet	-	-	-	0.15	0.76	0.19	-

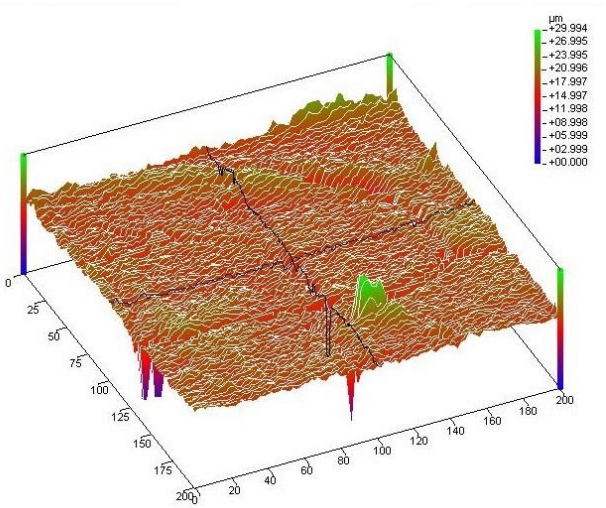

Figure 8 - Surface mapping of titanium plate coated with TiO_2 at 20V suspended in isopropanol based solution during 15 minutes obtained from non-contact optical profilometry

Characterisation of the samples by SEM reveals the microstructure formed from the deposited anatase particles. Figure 9 shows SEM images obtained from FTO coated glass, coated for 30s at 20V in acetylacetone based solution. The microstructure observed in this instance looked similar to that obtained on the other samples which were coated under different deposition conditions. This suggests that the significant differences responsible for the coating behaviour were macro structural.

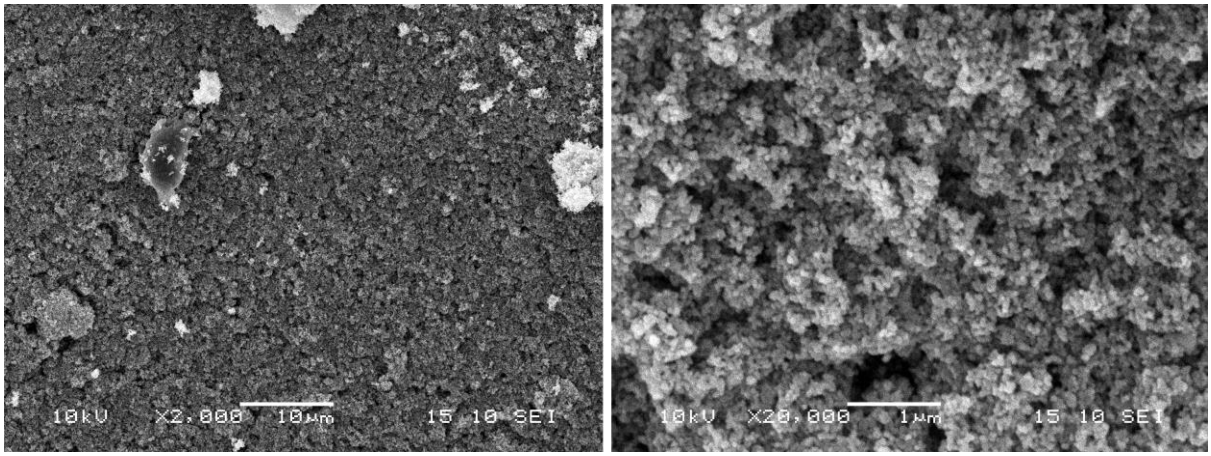

Figure 9 – Typical SEM images of TiO_2 electrophoretically deposited coatings on stainless steel at 20V for 30 seconds in isopropyl based solution.

f. Photocatalytic degradation of NO_2

The selected coatings were also tested in a reaction chamber coupled to a quadrupole mass spectrometer as shown in Figures 10a and 10b. To aid comparison values were normalised relative to the performance of an anatase P25 pellet. Figure 11 shows an example of both experiments for the FTO coated glass coated for 30s at 20V in acetylacetone based solution. Figure 12 shows the degradation for the active coatings and anatase pellet per mm^2 under a UV irradiation of wavelength (λ) 376-387nm. Figure 12 shows samples that were coated on FTO coated glass, in acetylacetone based solution at 20V for 30s and at 40V for 10s were extremely reactive. In comparison, stainless steel coated in acetylacetone based solution at 80V for 50s achieved the same performance as an anatase pellet.

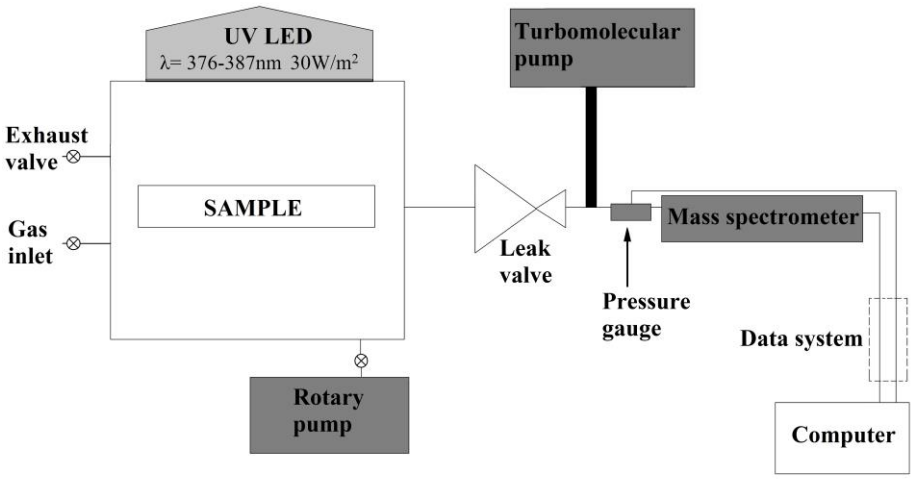

i)

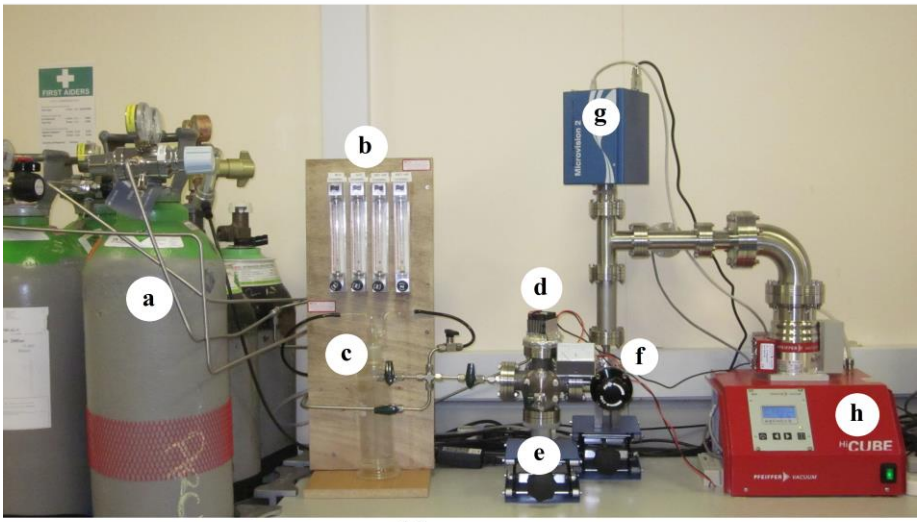

ii)

Figure 10 - i) Schematic design of the instrument used in this research. ii) Photograph of experimental setup. Labels on image as follows (a) gas bottles, (b) flow meters, (c) water bubbler, (d)

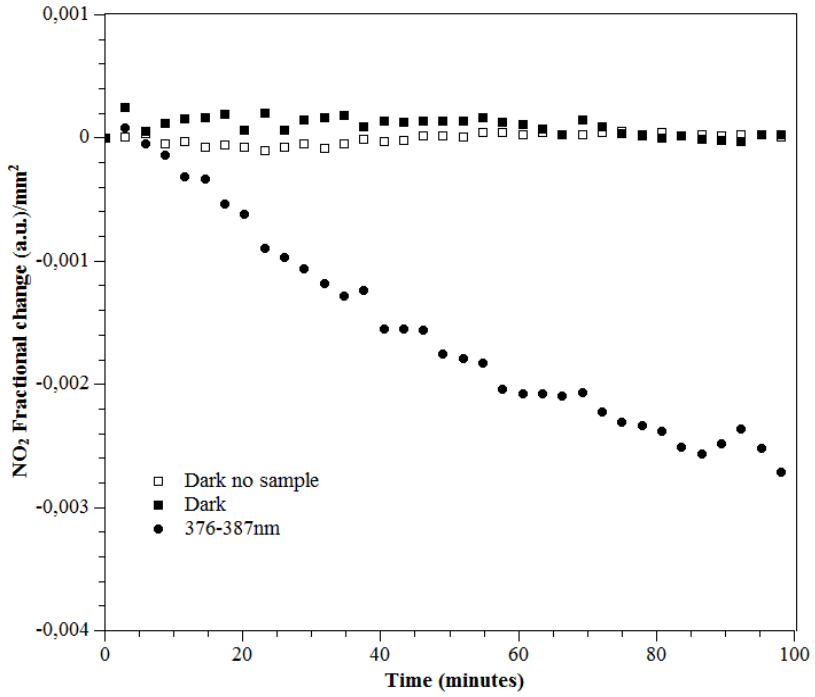

Figure 11 – NO_2 breakdown under 376-387nm carried by FTO coated glass coated at 20V during 30 seconds in acetylacetone based solution.

The highest efficiency photodegradation ratios were achieved from the coatings prepared on FTO coated glass. The two most active were formed at 20V for 30s at 40V for 10s in an acetylacetone based solution. The formation of O_2 and N_2 were observed during the photocatalytic reaction, detecting an increment of the O_2 peak, which indicates a reduction of NO_2 into N_2. The stoichiometric is not fully adjusted for O_2, since the O_2 peak is the convolution of species that contains oxygen, such as NO_2, CO_2, H_2O and O_2.

The differences in photocatalytic activity highlighted by Figure 12 indicate that the process of electrophoretic deposition can have a dramatic influence on the gaseous photocatalytic activity. The optical microscopy images (Figure 5) clearly show differences in the coating microstructure and the presence of varying degrees of surface cracking. It is likely that the presence of surface cracks increase the effective surface area of TiO_2 accessible to the UV irradiation and gases consequently improving influence performance. Figure 13 shows two high magnification SEM images which compare the compressed pellet and electrophoretic coating. Agglomerates of nanoparticles are clearly visible on the surface of the compressed pellet, shown in brighter contrast due to surface charging. It is widely accepted that nanoparticles aggregate due to electrostatic forces and would remain in this state during pressing of the pellet. In comparison, when introduced into a liquid, such as the electrolyte used for the deposition process, the particles can de-flocculate. The electrophoretic deposition process provides the

opportunity for the nano-particles to adopt a new structure with improved gas and light penetration resulting in a modified photo activity.

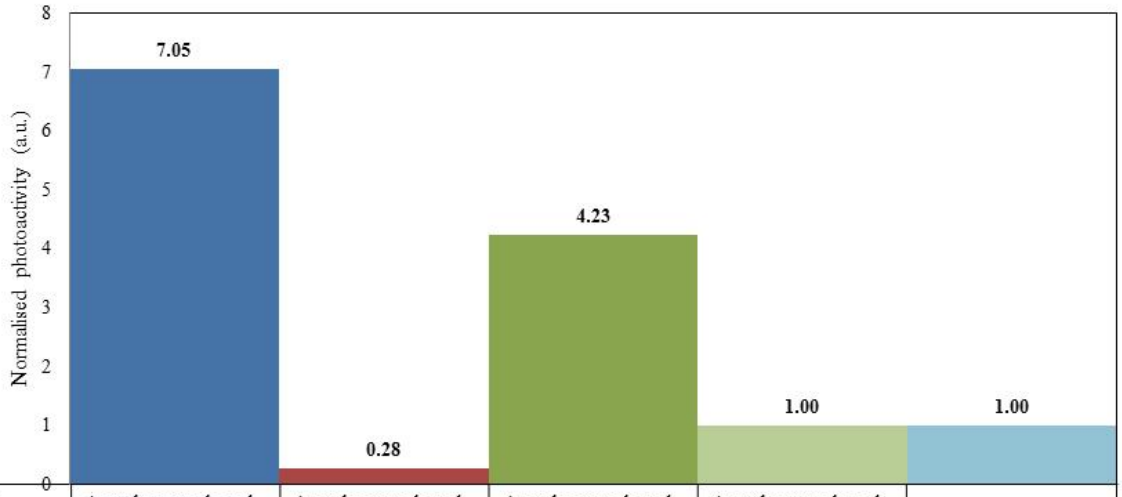

Solvent	Acetylacetone based solution	Acetylacetone based solution	Acetylacetone based solution	Acetylacetone based solution	
Voltage	20V	20V	40V	80V	
Time	30 seconds	50 seconds	10 seconds	50 seconds	
Substrate	FTO glass	FTO glass	FTO glass	Stainless steel	
Photoactivity	7.05	0.28	4.23	1.00	*1*
Picture (scale 500μm)	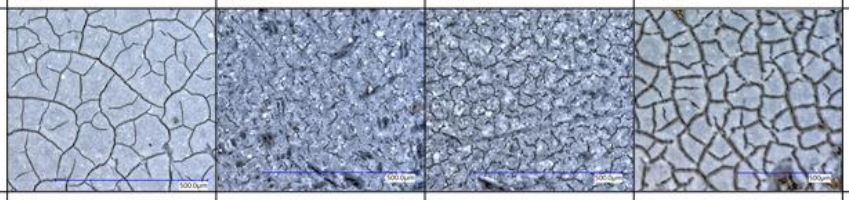				n/a
Thickness	16.4µ	12.2µ	7.3µ	22.3µ	n/a
Roughness	0.77µ	0.56µ	0.75µ	1.84µ	0.15µ

Figure 12 – Bar chart of NO_2 decomposition of 5 samples under 376-387nm for 100 minutes.

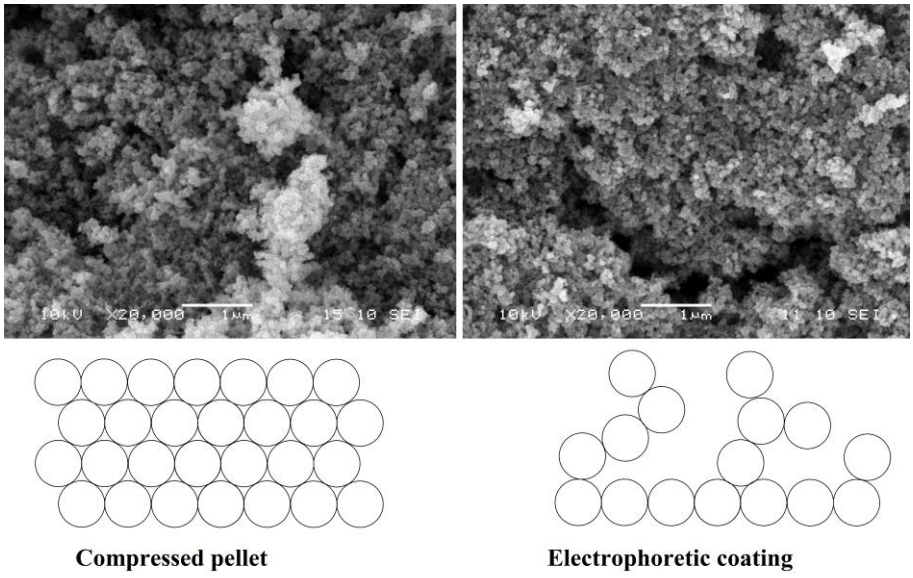

Figure 13 – Schematic explanation of the increment in surface area

Results indicate that the surface morphology at both nano and micro scales play an important role in influencing the photocatalytic performance. In particular these can be summarised as micro surface fractures, identified using digital microscopy in the 100μm range (Figure 5) and non-contact profilometry in the 2μm range (Figure 8 and Table 2); and nano surface fractures in the order of 0-200nm, identified by SEM (Figures 9 and 12).

4. Conclusions

The following conclusions can be drawn for the development of low-cost and large area photoactive coatings for pollution control:

(i) Electrophoretic deposition has been successfully demonstrated to produce TiO_2 anatase coatings on fluorine doped tin oxide (FTO) coated glass, stainless steel and titanium substrates. The most uniform and mechanically stable coatings were formed on the FTO coated glass due to the minimization on the stress caused by the thermal mismatch when the sample was calcined at 450ºC.

(ii) The surface characteristics of the coatings on each substrate material, in terms of mechanical stability, surface roughness and thickness were successfully controlled by varying the applied voltage between 20 and 80V, deposition time between 10 and 900s and electrolyte composition, which was either isopropanol or acetylacetone based.

(iii) Coatings produced using an applied voltage between 20 and 40V and exposure time less than 100s were uniform and mechanically stable suggesting these are optimal conditions.

(iv) The acetylacetone based electrolyte with a higher dielectric constant and lower viscosity provided better stability to the TiO_2 nano-particle suspension compared to the isopropanol based electrolyte and, performed particularly well for longer exposure times and higher voltages.

(v) The photocatalytic degradation of NO_2 was monitored using a quadrupole mass spectrometer, showing coatings deposited on FTO coated glass exhibited significantly higher photocatalytic activities compared to a press pellet; whilst also displaying good adhesion to the substrate and surface uniformity.

(vi) Micro and nano structural analysis of the coatings revealed that the thickness was not a determining factor influencing photocatalytic activity. It is postulated that introduction of nanoparticle agglomerates into the electrolyte allowed the individual particles to disperse thereby promoting the formation of a new nanostructure upon deposition, with improved photocatalytic performance.

Acknowledgement

The authors acknowledge support from the University of Bath research studentship and instrumentation funding from the Royal Society, Research grant RG110024. Thanks are also due to Professor W. N. Wang (University of Bath) for supplying the LEDs and Dr. S. Biswas from LMNIIT Jaipur (India) for electrophoretic coating facilities. In addition the authors wish to acknowledge the help of Guy Tolley and Keyence for images taken on the VHX-5000 Digital optical microscope. Thanks are also due to the UK India Education and Research Initiative (UKIERI-II) coordinated by the British Council, New Delhi, India, for financial support through a thematic partnership.

Bibliography

[1] S. Solomon, D. Qin, M. Manning, Z. Chen, M. Marquis, K.B. Averyt, M. Tignor, H.L. Miller, Contribution of Working Group I to the Fourth Assessment Report of the Intergovernmental Panel on Climate Change, 2007.

[2] Directive 2008/50/EC of the European Parliament and of the Council of 21 May 2008 on ambient air quality and cleaner air for Europe.

[3] A. Fujishima and K. Honda, Electrochemical photolysis of water at a semiconductor electrode, *Nature*, vol. 238, no. 5358, pp. 37–38, 1972.

[4] A. P. H. García and S. L. Suib, *Solar Photocatalysis for Environment Remediation, In New and Future Developments in Catalysis*, Elsevier. 2013.

[5] A. Z. Fujishima, Titanium dioxide photocatalysis: present situation and future approaches, *Comptes Rendus Chim.*, vol. 9, no. 5–6, pp. 750–760, 2006.

[6] A. Fujishima, T. N. Rao, and D. A. Tryk, Titanium dioxide photocatalysis, *J. Photochem. Photobiol. C Photochem. Rev.*, vol. 1, no. 1, pp. 1–21, 2000.

[7] O. Carp, C. L. Huisman, and A. Reller, Photoinduced reactivity of titanium dioxide, *Prog. Solid State Chem.*, vol. 32, no. 1–2, pp. 33–177, 2004.

[8] D. A. Tryk, A. Fujishima, and K. Honda, Recent topics in photoelectrochemistry: achievements and future prospects, *Electrochim. Acta*, vol. 45, no. 15–16, pp. 2363–2376, 2000.

[9] M. R. Hoffmann, S. T. Martin, W. Choi, and D. W. Bahnemann, Environmental applications of semiconductor photocatalysis, *Chem. Rev.*, vol. 95, no. 1, pp. 69–96, 1995.

[10] A. Heller, Chemistry and Applications of Photocatalytic Oxidation of Thin Organic Films, *Acc. Chem. Res.*, vol. 28, no. 12, pp. 503–508, 1995.

[11] M. Serratos and A. Bronson, The effect of oxygen partial pressure on the stability of Magneli phases in high temperature corrosive wear, *Wear*, vol. 198, no. 1–2, pp. 267–270, 1996.

[12] L. Kavan, M. Gratzel, S. E. Gilbert, C. Klemenz, H. J. Scheel, Electrochemical and Photoelectrochemical Investigation of Single-Crystal Anatase, *J. Am. Chem. Soc.*, vol. 118, no. 28, pp. 6716–6723, 1996.

[13] R. Asahi, Y. Taga, W. Mannstadt, and A. J. Freeman, Electronic and optical properties of anatase TiO_2, *Phys. Rev. B*, vol. 61, no. 11, pp. 7459–7465, 2000.

[14] T. A. Egerton and J. A. Mattinson, The influence of platinum on UV and ‘visible’ photocatalysis by rutile and Degussa P25, *J. Photochem. Photobiol. A Chem.*, vol. 194, no. 2–3, pp. 283–289, 2008.

[15] W.-C. Oh, F.-J. Zhang, and M.-L. Chen, Characterization and photodegradation characteristics of organic dye for Pt–titania combined multi-walled carbon nanotube composite catalysts, *J. Ind. Eng. Chem.*, vol. 16, no. 2, pp. 321–326, 2010.

[16] Y. H. Tseng and C. H. Kuo, Photocatalytic degradation of dye and NO(x) using visible-light-responsive carbon-containing TiO_2, *Catal. Today*, vol. 174, no. 1, pp. 114–120, 2011.

[17] G. K. Mor, O. K. Varghese, M. Paulose, K. Shankar, and C. A. Grimes, A review on highly ordered, vertically oriented TiO_2 nanotube arrays: Fabrication, material properties, and solar energy applications, *Sol. Energy Mater. Sol. Cells*, vol. 90, no. 14, pp. 2011–2075, 2006.

[18] M. J. Sampaio, C. G. Silva, R. R. N. Marques, A. M. T. Silva, and J. L. Faria, Carbon nanotube–TiO_2 thin films for photocatalytic applications, *Catal. Today*, vol. 161, no. 1, pp. 91–96, 2011.

[19] T. Ohno, T. Tsubota, K. Nishijima, and Z. Miyamoto, Degradation of Methylene Blue on Carbonate Species-doped TiO_2 Photocatalysts under Visible Light, *Chem. Lett.*, vol. 33, no. 6, pp. 750–751, 2004.

[20] C. Y. Lin, Y. K. Fang, C. H. Kuo, S. F. Chen, C.-S. Lin, T. H. Chou, Y.-H. Lee, J.-C. Lin, and S.-B. Hwang, Design and fabrication of a TiO_2/nano-silicon composite visible light photocatalyst, *Appl. Surf. Sci.*, vol. 253, no. 2, pp. 898–903, 2006.

[21] J. Zhu, J. Ren, Y. N. Huo, Z. F. Bian, and H. X. Li, Nanocrystalline Fe/TiO_2 visible photocatalyst with a mesoporous structure prepared via a nonhydrolytic sol-gel route, *J. Phys. Chem. C*, vol. 111, no. 51, pp. 18965–18969, 2007.

[22] F. Zhang, M. Chen, and W. Oh, Photoelectrocatalytic properties of Ag-CNT/TiO_2 composite electrodes for methylene blue degradation, *New Carbon Mater.*, vol. 25, no. 5, pp. 348–356, 2010.

[23] E. Alonso, I. Montequi, and M. J. Cocero, Effect of synthesis conditions on photocatalytic activity of TiO_2 powders synthesized in supercritical CO_2, *J. Supercrit. Fluids*, vol. 49, no. 2, pp. 233–238, 2009.

[24] A. Mills, C. Hill, and P. K. J. Robertson, Overview of the current ISO tests for photocatalytic materials, *J. Photochem. Photobiol. A Chem.*, vol. 237, pp. 7–23, Jun. 2012.

[25] M. Nuño, R. J. Ball, and C. R. Bowen, Study of solid/gas phase photocatalytic reactions by electron ionization mass spectrometry, *J. Mass Spectrom.*, vol. 49, no. 8, pp. 716–726, 2014.

[26] B. Tryba, P. Homa, R. J. Wróbel, and A. W. Morawski, Photocatalytic decomposition of benzo-[a]-pyrene on the surface of acrylic, latex and mineral paints. Influence of paint composition, *J. Photochem. Photobiol. A Chem.*, vol. 286, pp. 10–15, Jul. 2014.

[27] T. Maggos, J. G. Bartzis, M. Liakou, and C. Gobin, Photocatalytic degradation of NOx gases using TiO2-containing paint: A real scale study, *J. Hazard. Mater.*, vol. 146, no. 3, pp. 668–673, 2007.

[28] Q.-J. Geng, X.-K. Wang, and S.-F. Tang, Heterogeneous Photocatalytic Degradation Kinetic of Gaseous Ammonia Over Nano-TiO2 Supported on Latex Paint Film, *Biomed. Environ. Sci.*, vol. 21, no. 2, pp. 118–123, 2008.

[29] L. Hochmannova and J. Vytrasova, Photocatalytic and antimicrobial effects of interior paints, *Prog. Org. Coatings*, vol. 67, no. 1, pp. 1–5, 2010.

[30] J. Kolarik and J. Toftum, The impact of a photocatalytic paint on indoor air pollutants: Sensory assessments, *Build. Environ.*, vol. 57, no. 0, pp. 396–402, 2012.

[31] M. Baudys, J. Krýsa, M. Zlámal, and A. Mills, Weathering tests of photocatalytic facade paints containing ZnO and TiO_2, *Chem. Eng. J.*, vol. 261, pp. 83–87, Feb. 2015.

[32] K. Yoshida, K. Matsukawa, and T. Yano, Microstructure and mechanical properties of silicon carbide fiber-reinforced silicon carbide composite fabricated by electrophoretic deposition and hot-pressing, *J. Nucl. Mater.*, vol. 386–388, pp. 643–646, Apr. 2009.

[33] I. Corni, M. P. Ryan, and A. R. Boccaccini, Electrophoretic deposition: From traditional ceramics to nanotechnology, *J. Eur. Ceram. Soc.*, vol. 28, no. 7, pp. 1353–1367, 2008.

[34] A. R. Boccaccini and I. Zhitomirsky, Application of electrophoretic and electrolytic deposition techniques in ceramics processing, *Curr. Opin. Solid State Mater. Sci.*, vol. 6, no. 3, pp. 251–260, Jun. 2002.

[35] M.-S. Wu, D.-S. Chan, K.-H. Lin, and J.-J. Jow, A simple route to electrophoretic deposition of transition metal-coated nickel oxide films for electrochemical capacitors, *Mater. Chem. Phys.*, vol. 130, no. 3, pp. 1239–1245, Nov. 2011.

[36] K. Tada and M. Onoda, Electrophoretic deposition of conjugated polymer: Deposition from dilute solution and PEDOT coating effect, *Synth. Met.*, vol. 159, no. 9–10, pp. 851–853, May 2009.

[37] O. O. Van der Biest and L. J. Vandeperre, Electrophoretic deposition of materials, *Annu. Rev. Mater. Sci.*, vol. 29, no. 1, pp. 327–352, Aug. 1999.

[38] C. Kaya, F. Kaya, B. Su, B. Thomas, and A. R. Boccaccini, Structural and functional thick ceramic coatings by electrophoretic deposition, *Surf. Coatings Technol.*, vol. 191, no. 2–3, pp. 303–310, Feb. 2005.

[39] V. Firouzdor, J. Brechtl, B. Hauch, K. Sridharan, and T. R. Allen, Electrophoretic deposition of diffusion barrier titanium oxide coatings for nuclear reactor cladding applications, *Appl. Surf. Sci.*, vol. 282, pp. 798–808, Oct. 2013.

[40] M. Farrokhi-Rad and M. Ghorbani, Electrophoretic Deposition of Titania Nanoparticles in Different Alcohols: Kinetics of Deposition, *J. Am. Ceram. Soc.*, vol. 94, no. 8, pp. 2354–2361, Aug. 2011.

[41] W. Shan, Electrophoretic deposition of nanosized zeolites in non-aqueous medium and its application in fabricating thin zeolite membranes, *Microporous Mesoporous Mater.*, vol. 69, no. 1–2, pp. 35–42, Apr. 2004.

[42] S. M. A. Fateminia, R. Yazdani-Rad, T. Ebadzadeh, and S. Ghashghai, Effect of dispersing media on microstructure of electrophoretically deposited TiO_2 nanoparticles in dye-sensitized solar cells, *Appl. Surf. Sci.*, vol. 257, no. 20, pp. 8500–8505, Aug. 2011.

[43] J. Tabellion and R. Clasen, Electrophoretic deposition from aqueous suspensions for near-shape manufacturing of advanced ceramics and glasses—applications, *J. Mater. Sci.*, vol. 39, no. 3, pp. 803–811, 2004.

[44] I. Gurrappa and L. Binder, Electrodeposition of nanostructured coatings and their characterization—a review, *Sci. Technol. Adv. Mater.*, vol. 9, no. 4, p. 43001, 2008.

[45] L. Grinis, S. Dor, A. Ofir, and A. Zaban, Electrophoretic deposition and compression of titania nanoparticle films for dye-sensitized solar cells, *J. Photochem. Photobiol. A Chem.*, vol. 198, no. 1, pp. 52–59, Jul. 2008.

[46] F.-J. Zhang, M.-L. Chen, and W.-C. Oh, Photoelectrocatalytic properties and bactericidal activities of silver-treated carbon nanotube/titania composites, *Compos. Sci. Technol.*, vol. 71, no. 5, pp. 658–665, 2011.

[47] G.-S. Kim, H.-K. Seo, V. P. Godble, Y.-S. Kim, O.-B. Yang, and H.-S. Shin, Electrophoretic deposition of titanate nanotubes from commercial titania nanoparticles: Application to dye-sensitized solar cells, *Electrochem. commun.*, vol. 8, no. 6, pp. 961–966, Jun. 2006.

[48] A. R. Boccaccini, S. Keim, R. Ma, Y. Li, and I. Zhitomirsky, Electrophoretic deposition of biomaterials, *J. R. Soc. Interface*, vol. 7, no. Suppl 5, pp. S581–S613, Aug. 2010.

[49] H. Farnoush, J. A. Mohandesi, and D. H. Fatmehsari, Effect of Particle Size on the Electrophoretic Deposition of Hydroxyapatite Coatings: A Kinetic Study Based on a Statistical Analysis, *Int. J. Appl. Ceram. Technol.*, vol. 10, no. 1, pp. 87–96, Jan. 2013.

[50] G. Mohanty, L. Besra, S. Bhattacharjee, and B. P. Singh, Optimization of electrophoretic deposition of alumina onto steel substrates from its suspension in iso-propanol using statistical design of experiments, *Mater. Res. Bull.*, vol. 43, no. 7, pp. 1814–1828, Jul. 2008.

[51] E. M. Wong and P. C. Searson, ZnO quantum particle thin films fabricated by electrophoretic deposition, *Appl. Phys. Lett.*, vol. 74, no. 20, 1999.

[52] Y. Hara, J. R. S. Brownson, and M. A. Anderson, Fabrication of Thin-Films Composed of ZnO Nanorods Using Electrophoretic Deposition, *Int. J. Appl. Ceram. Technol.*, vol. 9, no. 1, pp. 115–123, Jan. 2012.

[53] X. Nie, A. Leyland, and A. Matthews, Deposition of layered bioceramic hydroxyapatite/TiO_2 coatings on titanium alloys using a hybrid technique of micro-arc oxidation and electrophoresis, *Surf. Coatings Technol.*, vol. 125, no. 1–3, pp. 407–414, Mar. 2000.

[54] C. O. Ayieko, R. J. Musembi, S. M. Waita, B. O. Aduda, and P. K. Jain, Structural and Optical Characterization of Nitrogen-doped TiO_2 Thin Films Deposited by Spray Pyrolysis on Fluorine Doped Tin Oxide (FTO) Coated Glass Slides, *Int. J. Energy Eng.*, vol. 2, no. 3, pp. 67–72, 2012.

[55] S. Peng, F. Cheng, J. Liang, Z. Tao, and J. Chen, Facile solution-controlled growth of $CuInS_2$ thin films on FTO and TiO_2/FTO glass substrates for photovoltaic application, *J. Alloys Compd.*, vol. 481, no. 1–2, pp. 786–791, Jul. 2009.